Available online at **www.joac.info**

ISSN: 2278-1862

Journal of Applicable Chemistry

2019, 8 (3): 1053-1065

(International Peer Reviewed Journal)

Synthesis and Characterization of Xanthan Gum based Nanoparticles for Colon Targeted Drug Delivery of Mesalamine

Tulika Malviya*, Shehala, Lalit Mohan Dwivedi, Sneha Joshi, Surabhi Gupta, and Vandana Singh

Department of Chemistry, University of Allahabad-211002, Uttar Pradesh, **INDIA**

Email: tulika4manan@rediffmail.com

Accepted on 4th April, 2019

ABSTRACT

A promising nanocarrier (XMA_{NP}) for mesalamine drug has been crafted by the cross-linking and self-assembly of xanthan gum and methacrylic acid. The optimum sample with maximum % cross linking and minimum % Equilibrium Swelling Ratio as well as drug release has been obtained by monitoring and optimizing the different parameters of the nanoparticle synthesis. The XMA_{NP} have been characterized with the help of FTIR, FESEM, and HR-TEM which revealed that the size of the nanoparticle lies in the range of 100-300 nm. Thermal degradation kinetics suggested that the cross linked nanoparticles have high thermal stability. The XMA_{NP} could effectively load mesalamine drug where it exhibited 65.43% encapsulation efficiency in 24 h time. The drug release from the matrix depended on the pH of the buffer medium as well as on the extent of cross linking. The greater release of drug in the pH of Lower Gastrointestinal Tract reflected that the drug release through XMA_{NP} can increase the bioavailability of the drug in colon.

Graphical Abstract

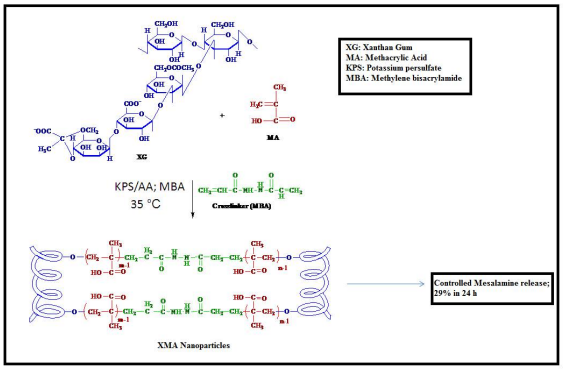

Keywords: Xanthan Gum, Nanoparticles, Methacrylate, Self assembly, Drug delivery.

INTRODUCTION

Current research in the field of nanotechnology has offered a wide variety of potential applications in various fields. As the size of a bulk material in the micro/macro range is converted into the nano

range, a number of special properties are exhibited by the material. Naturally available polysaccharides like Dextrin, Chitosan, etc., are communicated to act like a precursor for several industrial and medicinal applications such as sensors [**1, 2**], contrast agents [**3**], biofilm formation [**4**], anti-microbial activity [**5**] and drug delivery carriers [**6, 7**].The components used and the technique involved in its preparation plays a vital role in establishing the shape and size of the nanoparticle. Several physical and chemical methods are reported for the preparation of nanoparticles like nanoprecipitation [**8**], solvent dissolvation [**9**], emulsification [**10**], self-assembly [**6**] and free radical polymerization [**11**]. Among these, self assembly method is prominent as it does not involve the use of harsh chemicals, needs moderateexperimental conditions and enables the shielding of responsive materials [**12**]. The properties of the nanoparticles can also be tailored as required by changing various parameters of the method of preparation, viz. size of the nanoparticles can be controlled by the molecular weight and concentration of the precursor polysaccharide, compactness of the nanoparticles is influenced by the pH and ionic strength of the solvent, its polydispersity and zeta potential is changed by the concentration of the crosslinker [**13, 14**]. Therefore, the desired characteristics of the nanoparticles can be achieved by tuning different factors.

Xanthan gum (XG) is an abundant, naturally available and high-molecular weight polysaccharide ranging from 2×10^2 to 20×10^6 Da [**15**]. The primary, secondary and tertiary structural features make the XG highly stable, visco-elastic and lubricant gum [**16**]. However, its biodegradable nature lessens its applicability and thereby restricting its frequent use in various fields. Derivative materials of Xanthan gum have potential to be used for colon-targeted drug delivery through the oral administration [**17**] since they are vulnerable to biodegradation in the colon environment as well as its stability over a wide pH range. Xanthan gum can be modified by grafting which instigates hydrophobicity and steric bulkiness to the polysaccharide leading to the protection of the matrix and carbohydrate backbone. Methacrylic acid (MA) had been grafted onto XG using hydrogen peroxide–ferrous ammonium sulphate [**18**] initiator systems. However, no attempt has been made to prepare graft co-polymerized and crosslinked XG-*graft*-MA using potassium persulfate (KPS) and ascorbic acid (AA) as redox initiator system and methylene bisacrylamide (MBA) as crosslinker.

Upper gastrointestinal tract (GI) have a high pH which poses a serious challenge on oral colon drug delivery as the drug molecules are absorbed and degraded in the acidic environment. This leads to low bioavailability of the drug in the colon site providing an acute source of systemic side effects to the body. These drawbacks can be controlled by building colon-specific drug delivery carriers which are reported to be bacteria-dependent, time-dependent and pH dependent [**19**].The physiochemical properties of such material make them a suitable candidate for delivering the drug at the targeted site and thereby, improving the bioavailability and promising curative properties of the drug. Among these, the pH-dependent delivery carrier shows better practical applications and desirable properties due to the presence of acidic groups which limits its swelling in the acidic stomach fluid resulting into almost negligible release of the drugs from the matrix at low pH [**20**]. However, in the colon environment, high pH of the large intestine increases the extent of swelling of the matrix, causing the release of the drug where required [**21**].

In the present work reports the fabrication of MBA cross-linked XMA_{NP} nanoparticles via self-assembly method for colon-targeted drug delivery. Grafting and Crosslinking forms the root of the synthesis which controls the size, stability, and swelling behavior of XMA_{NP} nanoparticle. The improvement in its swelling behavior will, in turn, provide a pH-responsive character to the nanoparticle and ensure the sustained release of the model drug, mesalamine from the synthesized matrix.

MATERIALS AND METHODS

XG and Mesalamine were acquired from Himedia Company where XG was purified by precipitating with absolute ethanol. KPS and AA of Qualigens make were purchased while MA and MBA were of

LOBA Chemie. The replicability of the findings was confirmed by implementing all the experiments in triplicate.

The pH values of the buffer medium were corrected by using 5M HCl (GR, Merck, 35%); or 1M NaOH (Merck) with the help of pH meter (Lab tronics, model LT-49).Orbital shaker Incubator and Lyophilizer of Metrex Scientific Instruments (P) Ltd., New Delhi were used for the synthesis. Absorbance values were observed on UV/Vis Spectrophotometer (UV 100, Cyber lab, USA). FT-IR spectra were done with KBr pellets on FTIR Spectrum 2 Perkin Elmer Spectrophotometer in the range of 4000 to 400 cm^{-1}. The surface texture was recorded using a Nova Nano FE-SEM 450 (FEI) Field Emission Gun SEM and TEM (Tecnai G^2 20 (FEI) S-TWIN, FEI). SEM sample was prepared using double-stick carbon tape on aluminum stubs and gold coatings. XRD was carried out using an X-Ray Diffractometer (Panalytical X Pert Pro) at Cu/Kα-source. Thermogravimetric analysis was determined using STA 6000 (Perkin Elmeris) instrument under N_2 flow (50 mL min^{-1}) by raising the temperature at 20°C min^{-1}.

Standard drug stock solution was prepared by dissolving 0.32 mmol of Mesalamine in 500 mL of pH 7.4 phosphate buffer. Its standard calibration curve was hiked up playing on working standard solutions (20–0.1 mg mL^{-1}) which conformed to a correlation coefficient value (R^2) of 0.9999 by the linear regression analysis. The drug release study was carried out in Dissolution Rate Test Apparatus (Bezif Instruments Inc., Model: U.S.P./B.P.11.P. Std). The pH values of the gastrointestinal tract (GI) are taken for the study in order to access the effectiveness of the XMA_{NP} as a candidate for colon targeted drug delivery.

Synthesis of XMA_{Np}: XMA_{Np} nanoparticles were synthesized by redox initiated free radical polymerization and cross-linking method. Summarily, XG(4.0g) was dissolved in 1L of water and apt quantity of MA, KPS, and AA (Table 1) were added to the polysaccharide solution. The reaction system was exposed in the incubator shaker at 100 rpm and 35°Ctemperature. MBA was added to it after 1h and the reaction was further allowed for 4h. The copolymeric nanoparticles were precipitated with acetone and separated from concurrently formed poly(methacrylic acid)(PMA)by thoroughly washing with acetone. The solution was centrifuged for 5 min at 5500 rpm and lyophilized to get white, solid, fibrous $XMA_{NP.}$

The synthesis has been advanced by changing the concentrations of different process parameters. The % Yield and % cross linking were calculated by the following equations (Eq. 1, 2).

$$\text{Yield \%} = \frac{\text{Weight of resultant nanoparticles after freeze} - \text{drying}}{\text{Total weight of the reagents during synthesis}} \times 100 \quad \ldots (1)$$

$$\%\,C = \frac{\text{Weight of Copolymer} - \text{Weight of Polysaccharide}}{\text{Weight of monomer} + \text{Weight of crosslinker}} \times 100 \quad \ldots (2)$$

Measurements of equilibrium swelling capacity and swelling kinetics: The equilibrium swelling ratio (ESR) of XMA_{NP} (of varying % C) was assessed at 37°C in SGF (Simulated Gastric fluid) and SIF (Simulated Intestinal Fluid) solutions. 0.05 g of the samples was allowed to saturate and swell with respective buffers for 10 h to achieve the equilibrium swelling. After every 1 h, the swelled samples were phased out from the solution, wiped carefully and reweighed. The % ESR has been calculated using Eq. (3):

$$\text{ESR (\%)} = \frac{W_{eq} - W_d}{W_d} \times 100 \quad \ldots (3)$$

Where W_d and W_{eq} are weights of dried and swollen samples at equilibrium, respectively. The kinetics and rate parameter of swelling was calculated using the Voigt model (eq. 4)

$$S_t = S_e\left(1 - e^{-\frac{t}{\tau}}\right) \quad \ldots (4)$$

where S_t (g g^{-1}) is the swelling of the matrix at time t (min), S_e (g g^{-1}) is the equilibrium swelling, and τ (min) represents the rate parameter. Lower the rate parameter value (τ), higher will be the swelling rate [22].

In vitro drug delivery study

Determination of drug loading and entrapment efficiency: To evaluate the application of the nanoparticles in the delivery of Mesalamine drug, solvent swelling technique [23] was adopted. The loading of mesalamine was performed at pH 7.4 buffer solutions and 25°C for 12-24 h. In brief, XMA_{NP} (5 mg) was added in 20 mL of drug stock solution. The mixture was stirred in dark for 12 and 24 hand then centrifuged to settle down the suspended drug-loaded nanoparticle and decanted the supernatant solution. To remove the unloaded drug, the suspended XMA_{NP} was washed with 10 mL buffer solution for three times and was dried in a vacuum oven at 40 °C. The amount of drug loaded in XMA_{NP} was evaluated by measuring the difference of absorbance of supernatant and the standard solution of the drug by UV spectrophotometer at 303 nm (SGF) and 330 nm (SIF). The drug loading (%) and entrapment efficiency (%) were determined using the following Eq. 5,6.

$$\%\, Drug\ loading = \frac{Wt.\ of\ drug\ in\ sample}{Wt.of\ dried\ sample\ taken} \times 100 \quad \ldots (5)$$

$$\%\, Drug\ Entrapment\ Efficiency = \frac{Wt.of\ drug\ in\ sample}{Wt.of\ drug\ taken} \times 100 \quad \ldots (6)$$

Invitro Mesalamine delivery: In vitro release of Mesalamine from loaded XMA_{NP} was studied by dialysis process. Drug-loaded XMA_{NP} was kept in a dialysis membrane (12-14KDa, pore size 2.4 mm, Himedia) and dipped in 100 mL SGF buffer solution for 2 h followed by SIF in Drug Dissolution Apparatus at 37 ± 0.2°C. The membrane was allowed to rotate with the help of rotating paddle of the apparatus at 60 rpm up to 18 h. The amount of drug release was monitored by measuring the absorbance of the aliquots withdrawn from the buffer solutions after 1 h interval and was dropped back to the jars after each reading. The percentage of drug release was calculated applying the calibration curve for the respective pH buffer solutions (i.e. at SGF and SIF) obtained earlier. The study was done for the purified XG and different samples of XMA_{NP} at two pH values (SGF for 2 h followed by SIF) and the drug release profiles were plotted.

Various mathematical models such as zero order, first-order kinetic models, Korsemeyar–Peppas model, and Higuchi model were applied to study the kinetics and mechanism of the drug release.

RESULTS AND DISCUSSION

Synthesis of XMA_{NP}: The copolymeric XMA_{Np} nanoparticles were obtained by grafting of MA onto XG using KPS and MA redox system and subsequent crosslinking of the grafted chains with MBA. Various grades of the XMA_{Np} (XMA_{Np1} to XMA_{Np6}) were synthesized by varying the [MA] at fixed KPS/AA ratio (2:3) and [MBA] (2.5×10^{-2}M) at 35 ºC (Table 1). The effect of increasing [MA] was studied in the concentration range of 11×10^{-2} M to 27×10^{-2} M. The % C increased with the increase in [MA] (upto 23×10^{-2} M) as additional monomer molecules are available to bind with the polysaccharide, which however resulted to more homopolymer formation when the [MA] was >23×

10^{-2} M. 2:3 molar ratio of KPS/AA resulted into higher % C (45%) in comparison to 1:3(22%), which indicates that this redox ratio is more efficient to activate the XG backbone for immediate incorporation of the monomer. Therefore, the sample with maximum % C was obtained at 23×10^{-2} M of MA and 2:3 molar ratio of KPS/AA where the amounts of XG (0.1 g) and MBA (1.9×10^{-2} M) were fixed at 35°C.

Table 1. Optimization of reaction parameters for XMA_{Np} synthesis at fixed [MBA] = 1.9 X 10^{-2} and temperature (35°C).

S. No.	Sample	MA ($M \times 10^{-2}$)	$K_2S_2O_8$/AA (in Molar Ratio)	%Yield	% C	% ESR		Rate Parameter τ
						SGF	SIF	
1.	XMA_{NP1}	11	2:3	32.36	28.0	94	305	73.40
2.	XMA_{NP2}	15	2:3	41.51	32.9	75	280	74.52
3.	XMA_{NP3}	19	2:3	57.3	37.8	68	180	76.33
4.	XMA_{NP4}	23	2:3	62.4	44.9	61	135	81.76
5.	XMA_{NP5}	27	2:3	35.4	25.4	103	280	72.41
6.	XMA_{NP6}	23	1:3	30.5	22.1	124	300	70.85

Both XG and PMA are water-soluble macromolecules, while XMA_{Np} was insoluble and it has been reported [24] that polycarboxylic acids have a tendency to form interpolymer cross-linked complexes with water-soluble polysaccharides. The complexation of MA grafts and XG segments is vital for the hydrophobic driving force required to form nanoparticles.

Active free radical sites are generated on XG backbone on an interaction of KPS/AA redox system with water molecules. PMA chains are included in these active sites through free radical copolymerization [25]. This is followed by the subsequent addition of bifunctional monomer-MBA which plays a key role in crosslinking the PMA chains through covalent bonds resulting in the self-assembly of the molecules to form 'micelle' like nano aggregates. The presence of XG fragments in periphery prevented inter-particle crosslinking (Scheme-1). XMA_{Np} sample "XMA_{Np4}" was selected for further characterization as this is the sample of maximum % C.

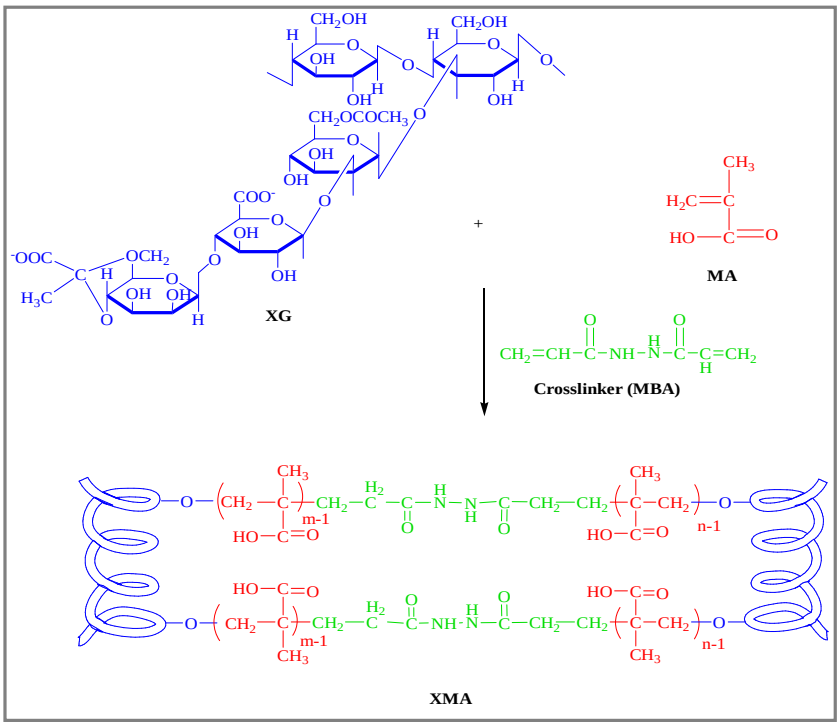

Scheme 1. A plausible route for the formation of XMA_{Np}

Characterization of XMA_{Np}

FTIR: FTIR spectra of XG showed a broad band at 3418 cm^{-1} attributed to the stretching vibrations of O-H groups, while the peak at 2898 cm^{-1} can be assigned to the stretching band of C-H groups (Figure 1). Peaks at 1726 cm^{-1} and 1415 cm^{-1} are attributed to the C=O group and symmetric carboxylate (COO^-) groups stretching vibrations of glucuronic acids respectively [**26, 27**].

FTIR spectra of XMA exhibited a significant shift and decrease in the intensity of stretching vibration at 3394 cm^{-1} which indicate that O-H groups have reacted with available bonding sites. The Peak at 2970 cm^{-1}indicates the presence of C-H groups at MA segments of XMA. The successful crosslinking of the grafts with MBA was confirmed by the 2^o amide (N-H) bending peak at 1529cm^{-1}. Drug-loaded XMA has a strong peak at 3426cm^{-1}due to overlapping stretching peaks of O-H (XG), NH_2 and phenolic O-H (drug). In addition, aromatic C=C stretching is visible as a pair of strong peaks between 1650 cm^{-1} - 1452cm^{-1}.

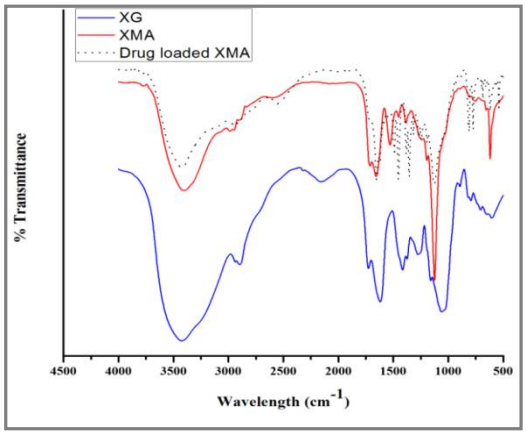

Figure 1. FTIR of XG, XMA_{Np4} and drug loaded XMA_{Np4}

SEM and TEM: The surface morphology of XG (Figure 2(A)) indicates the presence of layered and fibrous particles of variable size while the surface of XMA_{Np4} (Figure 2(B)) appeared rough, irregular, crosslinked, and aggregated. The presence of PMA segments atXMA_{Np4} can be manifested as the presence of small globular but agglomerated particles protruding out from XG surface which showed

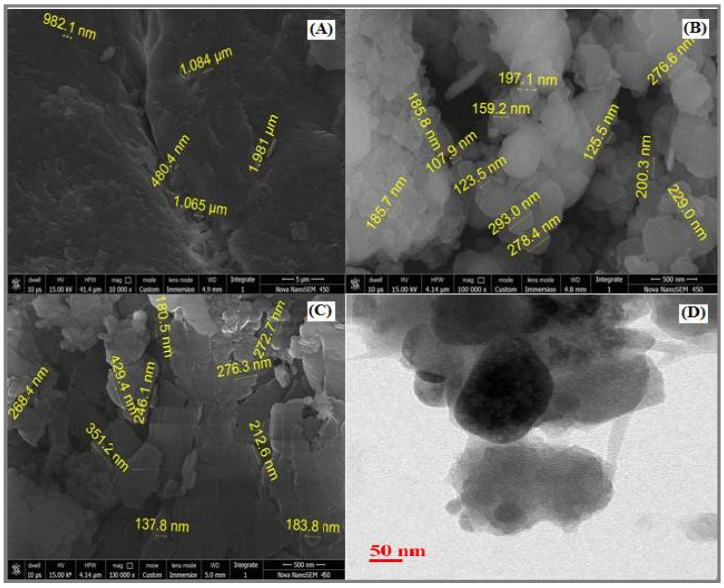

Figure 2. SEM micrographs of (A) XG, (B) XMA_{Np4}, (C) Drug loaded XMA_{Np4} at 100,000 magnifications while (D) TEM image of scattered XMA_{Np4} at 50 nm

a particle size ranging from 100-300 nm. The irregular and rough surface exhibited byXMA_{Np4} is likely to favor its drug loading capacity. Figure 2(C) shows the morphology of drug loaded XMA_{Np4} where the deposition of the drug at XMA_{Np4} surface is evident by the change in morphology from spherical, globular structure to layered crystals.

The morphology and size were also confirmed by the TEM image (Figure 2(D)) which revealed that the nanoparticles of XMA_{Np4} are well scattered and have small spherical shaped morphology in the diameter range of 100 to 300 nm.

XRD: XRD patterns (Figure 3) indicated that XG is amorphous in nature as it does not show crystalline peaks [**27**], while XMA illustrated significant, high ordered crystalline structure. It showed small as well as large diffraction peaks appearing at $2\theta = 28.18^o$, 29.79^o, 30.78^o and 35.77^o due to grafted MA onto XG.

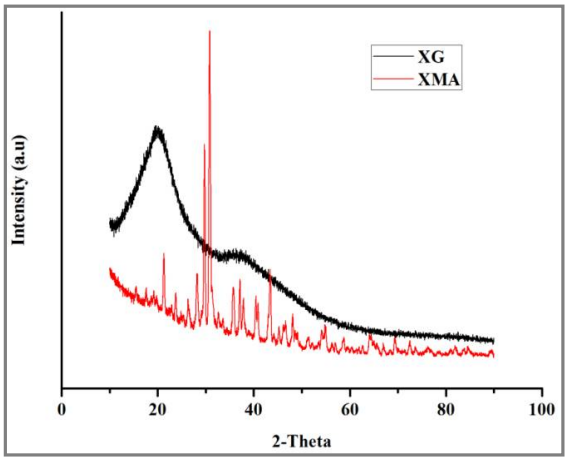

Figure 3. XRD of XG and XMA_{Np}.

TGA and DTG: Grafting of MA onto XG backbone affected the thermal stability of XG. Thermal analysis of XG showed two decomposition stages (Figure 4). The first DTG peak is visible at 91.83°C (initiated at ~27ºC and continued till 123ºC) which corresponded to ~13% weight loss due to evaporation of water molecules. The second DTG peak is at 299ºC (initiated from 205ºC and continued until 353ºC) which corresponded to ~42% weight loss due to break down of an unacetylated fragment of the polysaccharide backbone [**28**].

The TGA of XMA showed weight loss in four stages. First DTG peak can be seen at ~68ºC, corresponding to ~10%weight loss, due to the loss of moisture and adhered solvents. The second weightloss of 6% extends from 159 to 249 ºC and third peak centers around 313 ºC (between 271◦C and 327◦C), corresponding to 10% weight loss, indicated the loss of XG gum. Maximum 24% weight loss is seen between 331◦C and 423◦C, due to the loss of MA segments.

TGA of the drug-loaded sample has peaks shifted to a lower temperature which indicates the change in the degradation pattern of grafted XG. The first peak at 83.90 ºC is attributed to 8% weight loss due to the loss of adhered solvent. The peaks at 271ºC and 373ºC corresponded to loss of XG gum (16% weight loss between 151ºC and 287ºC) and MA segments (22% weight loss between 311ºC to 445ºC) respectively. The adsorbed drug species delayed the thermal degradation of MA than it was lost in the XMA itself indicating higher thermal stability. The thermogravimetric constants obtained (Table 2) further supports the analysis as higher values of Initial Decomposition Temperature (IDT), Maximum Rate Decomposition Temperature (MRDT), and Final Residue (FR) of XMA and drug-loaded XMA were obtained in comparison to XG.

Table 2. Thermogravimetric parameters of XG, XMA and drug loaded XMA

Samples	IDT	MRDT	FR
XG	27◦C	205◦C -353◦C	58%
XMA	30◦C	331◦C -423◦C	76%
Drug loaded XMA	29◦C	311◦C -445◦C	78%

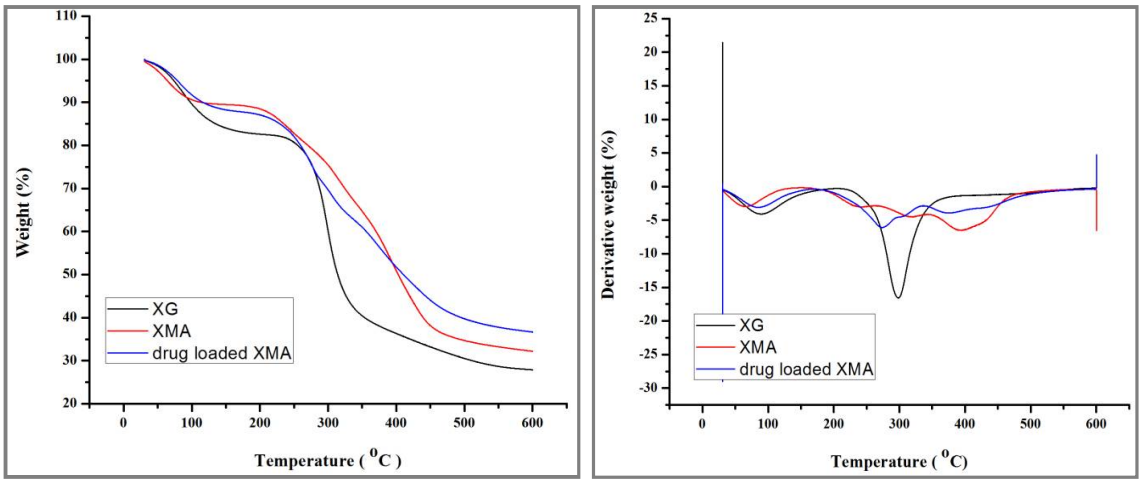

Figure 4. The thermograms of XG, XMA_{NP4} and drug loaded $XMA_{Np4.}$

Particle size analysis: The size of XMA_{NP4} was in the range of 193-500 nm, where 100% particles of XMA_{NP4}corresponded to a particle size of 418 nm (Figure 5). Polydispersity value for XMA_{NP4} was found to be 2 which indicate the heterogeneous distribution of the particles. Presence of greater percentage of smaller particles makes them possess adequate energy through the Brownian motion which prevents them from agglomeration.

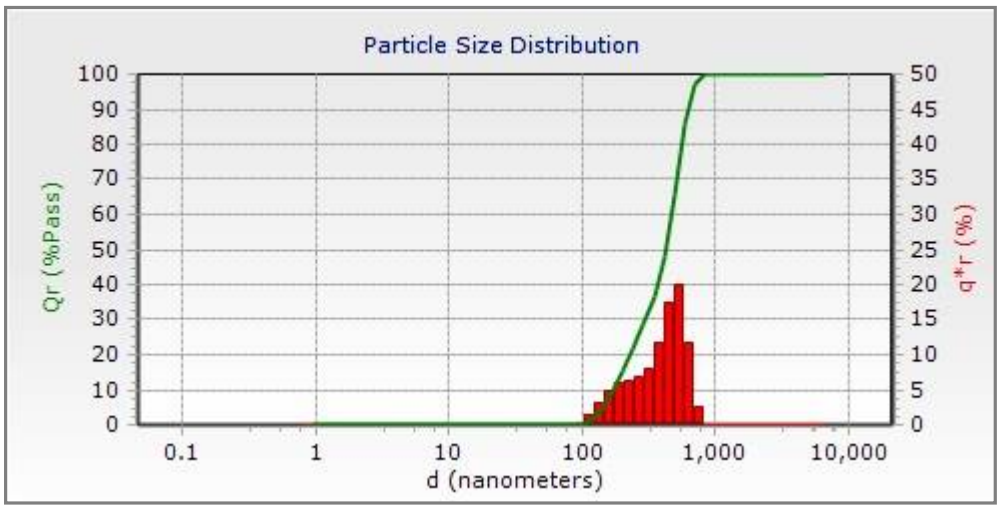

Figure 5. Particle size distribution of XMA_{NP4}.

Swelling study: The equilibrium swelling properties of XG and XMA_{Np} were investigated in SGF and SIF solutions at 37°C. XG exhibited the fundamental property of polysaccharide by dissolving in water and providing a homogeneous solution. This property is modified by grafting and crosslinking where the XMA_{Np} swelled in due course of time and the equilibrium swelling was established in ~7 h. The presence of PMA and MBA moieties in XMA_{Np} enhanced the hydrophilicity and facilitated the hydration as well as an expansion of the network. It was observed that % ESR decreased as %

Crosslinking increased and the minimum % ESR (61% at SGF and 170 % at SIF) was shown by the sample XMA_{Np4}which can be explained by its large surface area and structurally rigid nature due to highly crosslinked structure (Table 1).It is also evident from the swelling curve (Figure 6) that the swelling was initially fast which eventually retarded and attained an equilibrium swelling rate of ~7 h.

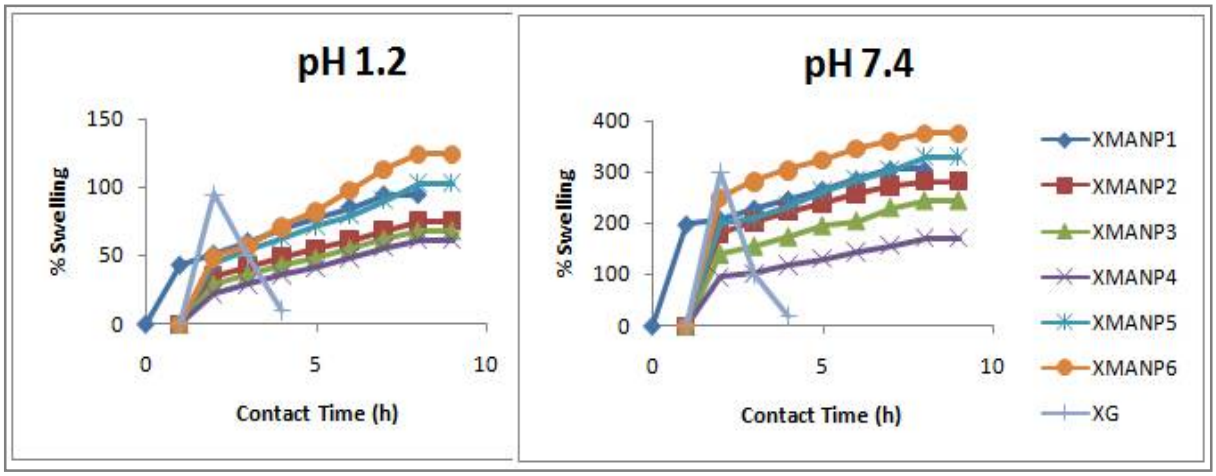

Figure 6. Swelling characteristics of XM and various XMA_{Np}at (a) SGF and (b) SIF.

The change in the texture of the nanoparticles from layered to porous fibres enhanced the swelling and water holding capacity of the molecules. Furthermore, XMA_{NP} showed a higher rate of swelling at SIF(than at SGF). The low swelling rate at SGF may be credited to the protonation of the hydrophilic groups at $XMA_{NP,}$ which opposed the interaction with water and thus lowered the swelling capacity. Whereas, at SIF, all the hydrophilic groups of XMA_{NP} backbone remained free to form H-bonding with the water molecules. Some of the –COOH groups of PMA may also ionize and the electrostatic repulsion between them, stretched the network widely, causing an enhancement of the swelling capacity.

APPLICATION

***In vitro* drug release studies:** The % loading of mesalamine drug into XMA_{NP} (after 12 and 24 h)is given in table 3. The maximum % loading and maximum % entrapment efficiency were achieved in 24 h. It was observed that the lower % swelling of XMA_{NP4} resulted in higher drug loading (65.43%) and entrapment efficiency (65.43%). The presence of COO- and OH- groups at the interaction sites within the XMA_{NP} matrix allowed hydrogen bonding/physical interactions with the drug molecule.

Table 3. Drug loading details of the tablet

Drug	Weight of XMA_{NP} (mg)	Weight of drug (mg)	Time of loading (h)	% of loading	% of encapsulation
Mesalamine	20	20	12 24	30.65 65.43	30.65 65.43

Identical experimental conditions were established for in-vitro drug release study and swelling study. As shown in Figure 7, mesalamine release was in accordance with the swelling kinetics of XMA_{NP}. The drug was solubilized and released as soon as XMA_{NP4}matrix swelled. Non swollen matrices retard the Mesalamine release which was very well exhibited by all the samples of XMA_{NP} resulting into slower drug release rate in both buffer mediums. In contrast, XG swelled very fast and 95% of the loaded drug was released in the first 9 h.

The Cumulative release (%) release of the drug loaded on XMA_{NP} was studied upto 18 h where for first 2 h, the sample was exposed to SGF subsequently followed by SIF. It was observed that in SGF, almost negligible swelling occurred due to which the drug was not released from the matrix. However, the drug molecules which could not be loaded effectively within the network of the matrix were seen to dissolve in the buffer medium [29]. At SIF, it was observed that as the percentage swelling of the matrix decreased, the drug was released in a more sustained manner. Maximum controlled drug release (~29% release after 12 h) behavior was shown by the sample XMA_{Np4} which well accorded with the high % C, low % ESR and high τ value. These results indicated XMA_{Np4}as the most suitable candidate for the controlled release of mesalamine drug as the higher amount of drug is released at the targeted site of the colon.

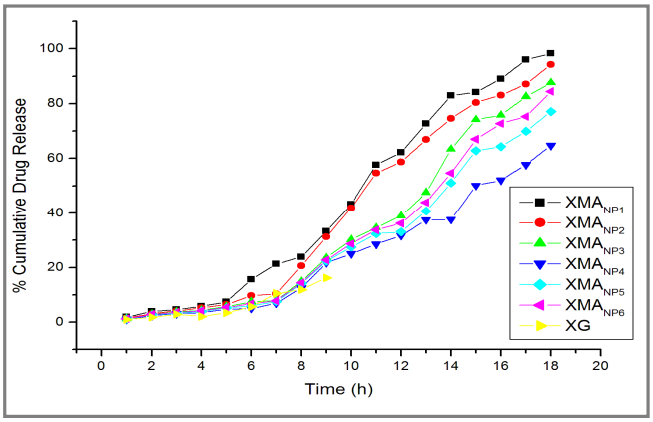

Figure 7. Mesalamine cumulative release (%) from XG and various samples of XMA_{NP} at pH gradient medium (2 h at SGF and upto 18h at SIF).

Kinetics and mechanism of Drug release: The kinetics of the drug release was studied by applying zero order [Eq. (7)], and first-order kinetic models [Eq. (8)].

$$Q_t = Q_0 + k_0 t \quad \ldots (7)$$

$$\log Q_t = \log Q_0 + \frac{k_1 t}{2.303} \quad \ldots (8)$$

where Q_0 is the initial amount of drug in tablet and Q_t is the amount of drug release at time t, k_0 and k_1 is the zero order and first order release constant expressed as concentration/time.

To investigate the release mechanism of $XMA_{Np,}$ the obtained data are fitted by two classical methods, Korsemeyer–Peppas mode [30][Eq. 9] and Higuchi model [31][Eq. 10].

$$\frac{M_t}{M_\infty} = kt^n \quad \ldots (9)$$

where M_t/M_∞ represents the fractional release of drug in time t, k is the rate constant and "n" shows the characteristic of the diffusion exponent of drug release. If the value of n is < 0.5, then the drug release process is controlled by Fickian diffusion; whereas, if n is > 0.5, non-Fickian diffusion mechanism is followed.

$$Q_t = Q_0 + k_H t^{1/2} \quad \ldots (10)$$

In the Higuchi model (Eq. 10),Q_0 is the initial amount of drug in solution, Q_t is the amount of drug released after time t, and k_H is the Higuchi dissolution constant. As shown in table 4, the drug release

profiles follow zero-order kinetics (with higher R^2 value). The value of n obtained for all the samples are greater than 0.5, which proposed that non-fickian diffusion mechanism is followed. Higher values of R^2 for the Higuchi model indicated that the drug is released from the matrix by the diffusion process.

Table 4. Kinetic data of XMA_{Np} at pH gradient

Nanoparticles	Zero order model R^2	First order Model R^2	Higuichi Model R^2	Korsemeyar-Peppas Model	
				n	R^2
XMA_{Np1}	0.943	0.733	0.998	0.542	0.998
XMA_{Np2}	0.896	0.682	0.984	0.551	0.988
XMA_{Np3}	0.850	0.624	0.961	0.622	0.959
XMA_{Np4}	0.944	0.665	0.992	0.779	0.986
XMA_{Np5}	0.846	0.576	0.959	0.787	0.948
XMA_{Np6}	0.961	0.870	0.920	0.757	0.963

CONCLUSION

The main idea of the present investigation was to formulate a colon-targeted drug delivery carrier utilizing a novel and biodegradable cross-linked nanoparticle of natural origin. The nanoparticles were prepared utilizing Xanthum Gum and Methacrylic acid via self-assembly method and were found to have porous and rough morphology. With an average diameter of ~150 nm and thermal stability, nanoparticles performed well as efficient drug delivery carrier for the mesalamine drug. The swelling capacity of the matrix was enhanced by its cross-linked network structure, which in turn, controlled the release of the confined mesalamine drug molecules at the targeted site of the colon. The drug release was apprehended by zero-order kinetic and non-Fickian diffusion mechanism.The nanoparticles displayed promising behavior for controlled release of mesalamine drug.

ACKNOWLEDGEMENTS

Dr. Tulika Malviyagratefully acknowledges financial support from SERB, New Delhi, India in the form of a research grant (No: SB/FT/CS-119/2012) and also to MRC, Malviya National Institute of Technology for the Spectral Analysis.

REFERENCES

[1]. A. Gaied, N. Jaballah, S. Teka, M. Majdoub, A Water-Insoluble β-Cyclodextrin Derivative for Hydroquinone Sensor Applications, *J. Applicable Chem.*, **2014**, 3(4), 1655-1664.
[2]. S. Pandey, G. K. Goswami, K. K. Nanda, Green synthesis of Polysaccharide/ Gold nanoparticle: An efficient ammonia sensor, *Carb. Pol.*, **2013**, 94(1), 229-234.
[3]. S. V. Raik, S. Andranovits, V.A. Petrova, Y. Xu, J. K. Lam, G. A. Morris, A.V.Brodskaia, L. Casettari, A. S. Kritchenkov, Y. A. Skorik, Comparative Study of Diethylaminoethyl-Chitosan and Methylglycol-Chitosan as Potential Non-Viral Vectors for Gene Therapy, *Pol.*, **2018**, 10(4), 442.
[4]. *B. Lu, F. Lu, L. Ran, K. Yu, Y. Xiao, Z. Li, F. Dai, D. Wu, G. Lan, Imidazole-molecule-capped chitosan–gold nanocomposites with enhanced antimicrobial activity for treating biofilm-related infections, J. Coll. and Inter. Sci.*, **2018**, 531, 269-281.
[5]. V. Singh, J. Singh, Preeti, A.K. Pandey, S. Joshi, L.M. Dwivedi, N. Fatima S. Tiwari, One Pot Catalyzed Synthesis of 1,3-bis (2-(4-hydroxyphenyl)-2-methyl-4,5- diphenyloxazol-3(2H)-yl) Thiourea and Its Antimicrobial Activity, *J. Applicable Chem.*, **2017**, 6(5), 688-700.
[6]. T. Malviya, S. Joshi, L. M. Dwivedi, K. Baranwal. Shehala, A. K. Pandey, V. Singh, Synthesis of Aloevera/Acrylonitrile based Nanoparticles for targeted drug delivery of 5-Aminosalicylic acid, *Inter. Jour. of Bio. Macromol.* **2017**, 17, 32877- 32885.

[7]. T. R. Hoare, D. S. Kohane, Hydrogels in drug delivery: Progress and challenges, *Poly.*, **2008**, 49, 1992-2007.
[8]. V. Singh, S. Joshi, T. Malviya, Carboxymethyl cellulose-rosin gum hybrid nanoparticles: An efficient drug carrier, *Inter. Jour. of Bio. Macromol.*, **2018**, 112,390–398.
[9]. K. Letchford, H. Burt, *A Review of the formation and classification of amphiphilic block copolymer nanoparticulate structures: micelles, nanospheres, nanocapsules and polymersomes, Euro. J. Pharma and Biopharm.*, **2007**, 65,259-269.
[10]. K. Nakabayashi, M. Kojima, S. Inagi, Y. Hirai, M. Atobe, Size-controlled synthesis of polymer nanoparticles with tandem acoustic emulsification followed by soap-free emulsion polymerization, *ACS Macro. Lett.*, **2013**, 2,482-484.
[11]. D.A. da Silva, J. P. A. Feitosa, H. C. B. Paula, R. C. M. de Paula, Synthesis and characterization of cashew gum/acrylic acid nanoparticles, *Mat. Sci. and Engin., C*, **2009**, 29,437-440.
[12]. B. Sarmento, A. J. Ribeiro, F. Veiga, D.C. Ferreira, R.J. Neufeld, Insulin-loaded nanoparticles prepared by alginate ionotropic pre-gelation followed by chitosan polyelectrolyte complexation, *J. Nano and Nanotech.*, **2007**, 7, 2833–2841.
[13]. S. Yang, Z. Tang, D. Zhang, M. Deng, C. Chen, PH and redox dual-sensitive polysaccharide nanoparticles for the efficient delivery of doxorubicin, *Biomat. Sci*., **2017**, 5(10), 2169-2178.
[14]. H. Jonassen, A.L. Kjoniksen, M. Hiorth, Effects of ionic strength on the size and compactness of chitosan nanoparticles, *Coll. and Pol. Sci.*, **2012**, 290,919–929.
[15]. R. Li, D.L. Feke, Rheological and kinetic study of the ultrasonic degradation of xanthan gum in aqueous solutions, *Food Chem.*, **2015**, 172,808–813.
[16]. N.M. Nikbakht, S.A. Goli, A. Nasirpour, Stability assessment of conjugated linoleic acid (CLA) oil-in-water beverage emulsion formulated with acacia and xanthan gums, *Food Chem.*, **2016**, 199(199), 258–264.
[17]. H. Shariful, Md. Moghal, M. Mizanur, A. H. M. Rahman, R. Masbahur, A. S. Shamsur Comparative studies of release profile of sustain release carvediol matrix tablets using methocel K100LV CR, methocel K100M CR and xanthum gum polymer, *Wor. J. Pharm. Sci.*, **2015**, 3(9), 1801-1811.
[18]. R. Kumar, A. Srivastava, K. Behari, Graft copolymerization of methacrylic acid onto xanthan gum by Fe^{2+}/H_2O_2 redox initiator, *Jour. of App. Pol. Sci.*, **2007**, 105,1922–1929.
[19]. M. George, T.E. Abraham, pH sensitive alginate–guar gum hydrogel for the controlled delivery of protein drugs, *Inter. J. Pharm.*, **2007**, 335, 123–129.
[20]. D. S. Sathya, M. Prabaharan, Guar gum succinate as a carrier for colon- specific drug delivery, *Inter. J. Bio. Macromol.*, **2016**, 84, 10–15.
[21]. H. Yihong, Y. Huiqun, X. Chaobo, pH-sensitive cationic guar gum/poly(acrylic acid) polyelectrolyte hydrogels: Swelling and in vitro drug release, *Carb. Pol.*, **2007**, 69,774–783.
[22]. T. S. Anirudan, S. Sandeep, P. L. Divya, Synthesis and characterization of maleated cyclodextrin-grafted-silylated montmorillonite for the controlled release and colon specific delivery of tetracycline hydrochloride, *RSC Adv.*, **2012**, 2, 9555-9564.
[23]. D. S. Hsieh, Controlled release Systems: Fabrication Technology, CRC Press, Inc., Boca Raton, Florida, vol. I. **1987**.
[24]. V. V. Khutoryanskiy, G. A. Mun, Z. S. Nurkeeva, A.V. Dubolazov, Interpolymer complexes of water-soluble nonionic polysaccharides with polycarboxylic acids and their applications, *Pol. Inter.*, **2004**, 53, 1382–1387.
[25]. V. Singh, A.K. Sharma, D.N. Tripathi, R. Sanghi, Poly(methylmethacrylate) grafted chitosan: An efficient adsorbent for anionic azo dyes, *J. Hazard. Mat.*, **2009**, 161, 955-966.
[26]. S. Maity, B. Sa, Ca-carboxymethyl xanthan gum mini-matrices: swelling, erosion and their impact on drug release mechanism, *Inter. Jour. of Bio. Macromol.*, **2014**, 68, 78–85.
[27]. S. Pandey, J. Ramontja, Rapid, facile microwave-assisted synthesis of xanthan gum grafted polyaniline for chemical sensor, *Inter. J. Bio. Macromol.*, **2016**, 89, 89–98.

[28]. C. Peniche, W. Arguelles-Monal, N. Davidenko, R. Sastre, A. Gallardo, J. San Roman, Self-curing membranes of chitosan/PAA IPN_S obtained by radical polymerization: preparation, characterization and interpolymer complexation, *Biomat.*, **1999**, 20(20), 1869-1878.
[29]. S. S. Vaghani, M. M. Patel, C. S. Satish, Synthesis and characterization of pH-sensitive hydrogel composed of carboxymethyl chitosan for colon targeted delivery of ornidazole, *Carb. Res.*, **2012**, 347, 76-82.
[30]. R. W. Korsemeyer, R. Gurny, E. Doelker, P. Buri, N. A. Peppas, A mechanism on solute release from porous hydrophilic polymers, *Intern. J. Pharm.*, **1983**, 15, 25-35.
[31]. T. Higuchi, Rate of release of medicaments from ointment bases containing drugs in suspension, *J. Pharm. Sci.*, **1961**, 50, 874-875.